

Article

Annealing Temperature-Dependent Effects of Fe-Loading on the Visible Light-Driven Photocatalytic Activity of Rutile TiO₂ Nanoparticles and Their Applicability for Air Purification

Soong Yeon Kim ¹, Shahid Saqlain ¹, Byeong Jun Cha ¹, Shufang Zhao ¹, Hyun Ook Seo ^{2,*} and Young Dok Kim ^{1,*} 

¹ Department of Chemistry, Sungkyunkwan University, Suwon 16419, Korea; sykim086@naver.com (S.Y.K.); shahidSaqlain@hotmail.com (S.S.); ckqudwins223@gmail.com (B.J.C.); taylorbjt@163.com (S.Z.)

² Department of Chemistry and Energy Engineering, Sangmyung University, Seoul 03016, Korea

* Correspondence: hyun.ook.seo@smu.ac.kr (H.O.S.); ydkim91@skku.edu (Y.D.K.);
Tel.: +82-010-3555-3164 (H.O.S.); +82-010-9163-8045 (Y.D.K.)

Received: 29 May 2020; Accepted: 1 July 2020; Published: 3 July 2020



Abstract: Commercial rutile TiO₂ particles (200–300 nm) were modified by the temperature-regulated chemical vapor deposition (tr-CVD) of Fe-oxide and subsequent annealing at various temperatures (300~750 °C). As a result of the modification, the photocatalytic activity of the TiO₂ regarding acetaldehyde removal under visible light was enhanced, and the enhancement effects were dependent on the annealing temperature. Specifically, the enhancement effects of the modification were most pronounced when Fe-TiO₂ was annealed at 375 °C, whereas the effects were significantly reduced by annealing at higher temperatures (525 and 750 °C). The analytical results with various techniques, including two surface-sensitive methods (XPS (X-ray photoelectron spectroscopy) and TOF-SIMS (time of flight-secondary ion mass spectrometry)), revealed that the stronger metal support interaction between TiO₂ and the loaded Fe-oxide at high temperature (>375 °C) resulted in the decreased charge separation efficiency and photocatalytic activity of the Fe-TiO₂ under light irradiation. The production scale for the Fe-TiO₂ photocatalysts can be easily increased (from 200 g to 8 kg per the unit process) by upsizing the reactor volume. The mass-produced samples exhibited similar activity to the samples produced at small scale, and they were photocatalytically active after being spread on a cement block (stainless steel plate) using a surface hardening agent (paint), showing the high applicability in real applications.

Keywords: iron oxide; rutile TiO₂; visible light-responsive photocatalyst; acetaldehyde

1. Introduction

The photocatalytic removal of harmful organic compounds in either the aqueous or gas phase has been studied extensively [1–6]. When the surface of a semiconductor is exposed to light whose energy exceeds the band gap of the semiconductor, electron-hole pairs can be generated upon the absorption of the light energy by the semiconductor. The light-induced electron-hole pairs can interact with O₂ and H₂O molecules at the surface of the semiconductor, generating strong oxidizing agents such as O₂^{•−} and OH radicals, respectively. These oxidizing agents can interact with other organic compounds on the surface, oxidizing them into less harmful species, e.g., CO₂ and H₂O, by total oxidation.

Acetaldehyde is in the class of volatile organic compounds (VOCs) that have been blamed for adverse effects on human health [7–11]. The photocatalytic removal of acetaldehyde using semiconducting materials has been studied by many research groups [12–15]. Among semiconducting

materials, anatase TiO₂ has been the most popular choice as a photocatalyst due to its non-toxicity, high chemical stability, and photocatalytic activity [16–19]. However, anatase TiO₂ can be used effectively as a photocatalyst only under UV light but not under visible light, due to its wide band gap (~3.2 eV). The portions of UV light in sunlight at the surface of the earth and in light from indoor lamps are limited. Thus, the wide band gap of anatase TiO₂ hampers its applicability as a photocatalyst for indoor and outdoor air purification.

The modification of TiO₂ with non-metal or metal ion doping has been investigated very extensively by many research groups to develop visible-light-responsive photocatalysts based on TiO₂ [20–24]. The loaded dopant can provide additional electronic states between the original band gap of TiO₂ so that the modified TiO₂ can utilize visible light to generate light-induced electron-hole pairs that can initiate the photocatalytic process. It is a general belief that rutile TiO₂ is less advantageous than anatase TiO₂ due to the shorter lifetime of its induced electron-hole pairs. However, rutile TiO₂ exhibits a smaller band gap (~3.0 eV) than anatase TiO₂, which makes rutile TiO₂ a possible candidate base material for developing visible-light-responsive photocatalysts [25–27]. Recently, we demonstrated that the anatase-to-rutile phase transition of commercial TiO₂ particles (P25, Evonik), which originally consisted of both anatase and rutile phases in an 8:2 ratio, could enhance the photocatalytic activity regarding acetaldehyde oxidation under visible light irradiation [28]. The anatase-to-rutile transformation was achieved by thermal annealing at 750 °C, and the visible-light response of the rutile TiO₂ can be further enhanced by the small loading of Fe-oxide via the temperature-regulated chemical vapor deposition (tr-CVD) [28]. Previous results also showed that the amount of Fe-loading was an important factor in determining the photocatalytic activity of Fe-loaded rutile TiO₂ under visible light, since the formation of larger Fe-oxide particles on the surface of TiO₂ can facilitate the non-radiative recombination of light-induced electron-hole pairs [28].

In this work, we investigated the annealing temperature dependency of the enhancement effects of a small Fe-loading (0.4 wt%) on the photocatalytic activity of rutile TiO₂ towards acetaldehyde removal under visible light irradiation. Commercially available alumina-coated rutile TiO₂ particles (200–300 nm) produced via a sulfuric acid process and commonly used as a pigment in coloring processes were chosen as a starting material for the modification. These TiO₂ particles are widely used due to their high refractive index, giving a high hiding power in white paints, and also as UV-protection agents in various composite materials; however, these TiO₂ particles are known to have very little photocatalytic activity. It is notable that these TiO₂ materials are well known to be cost-effective, so giving photocatalytic activity to these commercially available rutile TiO₂ materials with a slight surface modification would accelerate the wide application of photocatalysts. A very small amount of Fe-oxide (0.4 wt%) was loaded on the rutile TiO₂, and the Fe-loaded TiO₂ particles were annealed at various temperatures in the range of 300–750 °C. We found that there was an optimum temperature (375 °C) of annealing for the maximization of the enhancement effects of Fe-loading. Various analyses, including by two surface sensitive techniques (XPS (X-ray photoelectron spectroscopy) and TOF-SIMS (time of flight-secondary ion mass spectrometry)), revealed that the stronger metal support interaction between TiO₂ and the loaded Fe-oxide at higher temperature (>375 °C) can reduce the charge separation efficiency and the photocatalytic activity of Fe-loaded rutile TiO₂ under light irradiation. In addition, the feasibility of the mass production of Fe-modified rutile TiO₂ and its applicability in outdoor and indoor air purification were also examined.

2. Results and Discussion

2.1. Characterization

The amount of Fe-loading in TiO₂ particles was determined to be 0.4 wt% by ICP-OES analysis. Figure 1a–c show TEM images of three samples (TiO₂, and Fe-TiO₂-375 and -750). In all three cases, the TiO₂ particles were hexagonal in shape, with a size range of 200–300 nm. Any changes in the structure of the TiO₂ particles upon Fe-loading and annealing were not noticeable in the TEM images,

which can be attributed to the very small amount of Fe-loading (0.4 wt%) on the TiO₂ particles. The crystallinities of all the synthesized samples (Fe-TiO₂-300, -375, -450, -525, and -750) were examined by obtaining their XRD patterns. Figure 1d shows the XRD patterns of three samples (TiO₂, and Fe-TiO₂-375 and -750) and pristine TiO₂ (a comparison of the XRD patterns of all the synthesized samples and pristine TiO₂ can be found in Supporting information). All the XRD patterns were almost identical to those of pristine TiO₂ and were well matched with the standard rutile phase TiO₂ spectrum (JCPDS No. 88-1174), and other peaks related to anatase or brookite TiO₂ were not observed. This indicated that no phase transformations of TiO₂ took place, and the loading amount of Fe was too small to be detected in the XRD analysis.

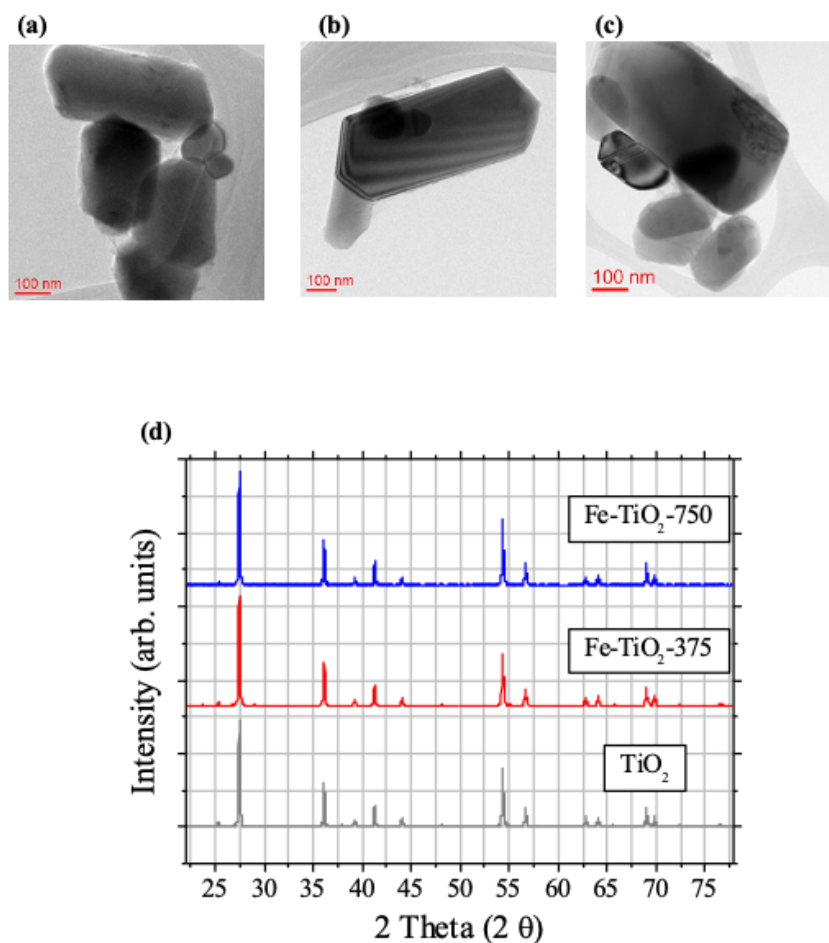


Figure 1. Characterization results for TiO₂, Fe-TiO₂-375, and Fe-TiO₂-750 particles. TEM images of (a) TiO₂, (b) Fe-TiO₂-375, and (c) Fe-TiO₂-750 particles. (d) XRD patterns of TiO₂, Fe-TiO₂-375, and Fe-TiO₂-750 particles (XRD patterns of all the synthesized samples are provided in Supporting information).

The specific Brunauer–Emmett–Teller (BET) surface areas of all the synthesized samples and pristine TiO₂ were examined (Supporting information), and Table 1 shows the specific BET surface areas of three samples (TiO₂, and Fe-TiO₂-375 and -750). The surface area of TiO₂ gradually decreased as the annealing temperature was increased from 375 to 750 °C after Fe-loading. However, only a marginal decrease in the surface area of the TiO₂ was observed (from 15.1 to 11.8 m²/g), even after the 750 °C annealing following the Fe-loading.

Table 1. The specific Brunauer–Emmett–Teller (BET) surface areas of TiO₂, Fe-TiO₂-375, and Fe-TiO₂-750 particles (the specific BET surface areas of all the synthesized samples are provided in Supporting information 1).

	TiO ₂	Fe-TiO ₂ -375	Fe-TiO ₂ -750
Specific BET surface area (m ² /g)	15.1	13.8	11.8

2.2. Photocatalytic Removal of Acetaldehyde

The photocatalytic degradation of gaseous acetaldehyde under visible light irradiation was carried out with TiO₂ and Fe-TiO₂-300, -375, -450, -525, and -750, and the results are shown in Figure 2. The experiments were carried out with a drop-casted film consisting of pristine TiO₂ and the synthesized Fe-TiO₂ samples prepared by a drop-casting method (the experimental details can be found in Section 3.3.). Scanning tunneling microscopic (SEM) analysis revealed that each drop-casted film consisted of individual TiO₂ particles without noticeable agglomeration among the particles, indicating that the individual TiO₂ particles were almost intact after the drop-casting process (Supporting information).

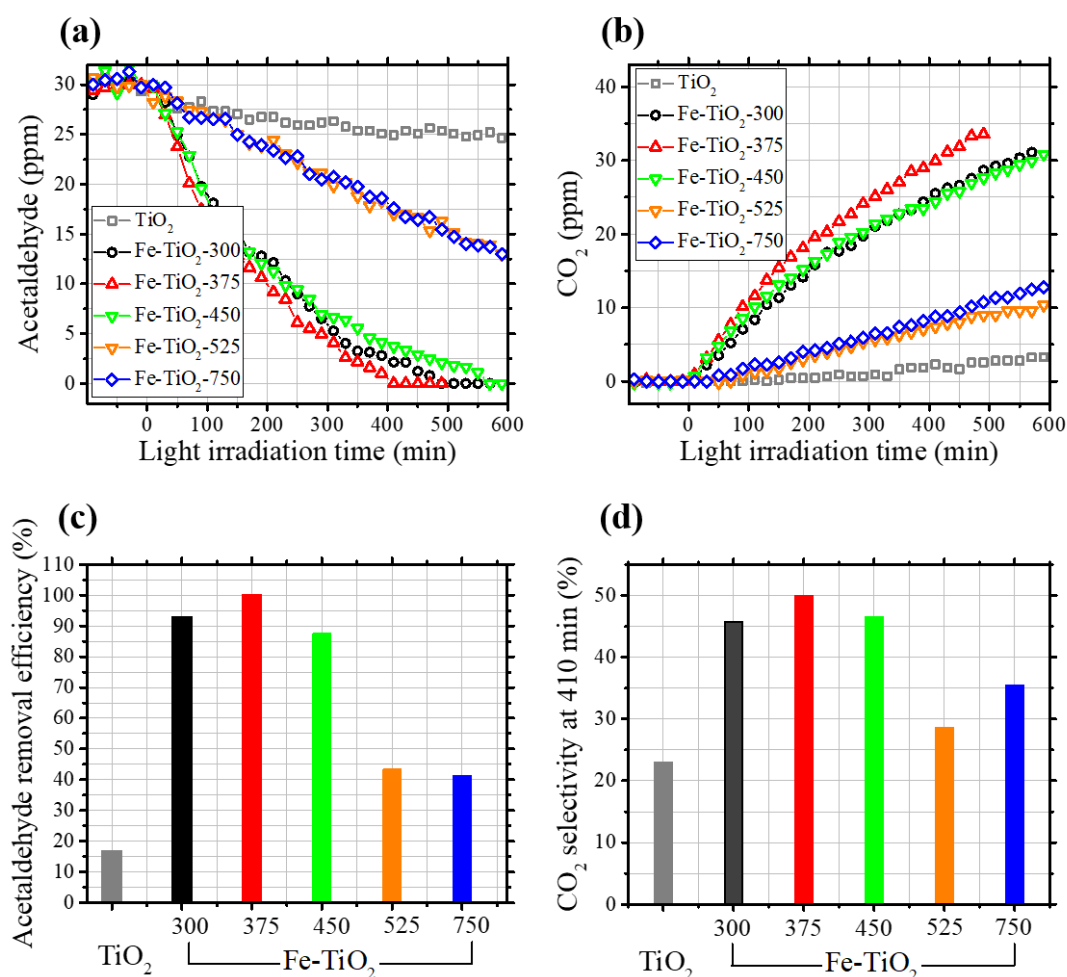


Figure 2. Results of the photocatalysis experiments. Concentration changes of (a) acetaldehyde and (b) CO₂ as a function of the visible light irradiation time in the presence of as-received TiO₂ (TiO₂) and five different Fe-TiO₂ samples (Fe-TiO₂-300, -375, -450, -525, and -750). (c) Removal efficiencies for acetaldehyde and (d) CO₂ selectivity determined after 410 min of visible light irradiation in the presence of TiO₂ and Fe-TiO₂-300, -375, -450, -525, and -750.

Figure 2a,b show the concentration changes of acetaldehyde and CO₂ during the photocatalysis experiments under visible light irradiation. The negative time scales correspond to the pre-adsorption stage in the dark, which was performed prior to the photocatalysis experiments. No notable changes in the concentration of acetaldehyde were observed for any of the TiO₂ samples (TiO₂ and Fe-TiO₂-300, -375, -450, -525, and -750) at the pre-adsorption stage, indicating that the adsorption of acetaldehyde in the dark was negligible for all the cases of the samples.

Upon the visible light irradiation of the surface of all the samples, the concentration of acetaldehyde started to decrease, and that of gaseous CO₂ increased without an induction time, showing that the photocatalytic removal of acetaldehyde took place (Figure 2a,b). It is clear that the photocatalytic activity of TiO₂ in terms of acetaldehyde removal and CO₂ evolution under visible light irradiation was enhanced upon Fe-loading, irrespective of the annealing temperature within the range of 300 to 750 °C (Figure 2a,b). However, the enhancement effects of Fe-loading on the photocatalytic activity of TiO₂ under visible light depended on the annealing temperature. Almost all of the gaseous acetaldehyde molecules in the reactor were removed by three Fe-TiO₂ samples (Fe-TiO₂-300, -375, and -400) after 590 min of blue light irradiation (Figure 2a). By contrast, only roughly half of the acetaldehyde molecules were removed by Fe-TiO₂ samples annealed at higher temperatures (Fe-TiO₂-525 and -750) under the same experimental conditions (Figure 2a).

One might note that the evolution of CO₂ continued even after all the gaseous acetaldehyde molecules in the reactor were removed. For instance, in the presence of Fe-TiO₂-375 samples, the concentration of gaseous CO₂ continued to increase even after 410 min when the acetaldehyde concentration in the reactor reached zero (Figure 2a,b). This phenomenon can occur when gaseous acetaldehyde is first removed by partial oxidation on the surface of a photocatalyst, and the partially oxidized species is later oxidized into CO₂ by a longer exposure to light [28–30]. The formation of acetic acid as an intermediate species on the surface of photocatalysts during the photocatalytic oxidation of acetaldehyde into CO₂ was previously reported [28–30]. The previous results indicated that the reaction rate of acetic acid oxidation into CO₂ was slower than that of acetic acid formation from acetaldehyde, which can result in the CO₂ selectivity being higher than 100% at longer reaction times [28–30].

The concentration change of acetaldehyde during each photocatalysis experiment was further examined by obtaining the C/C₀ value (%) for acetaldehyde and the acetaldehyde removal efficiency (%) for each duration of light irradiation. The C/C₀ value (%) for acetaldehyde was calculated as follows in Equation (1):

$$\frac{\text{Acetaldehyde concentration measured with each sample at each time}}{\text{Acetaldehyde concentration measured without sample}} \times 100 = \frac{C}{C_0} \times 100 (\%) \quad (1)$$

The acetaldehyde removal efficiency (%) for each irradiation duration was determined as follows in Equation (2):

$$\left(1 - \frac{C}{C_0}\right) \times 100 (\%) \quad (2)$$

For this calculation, the C/C₀ of each sample at each time was used. Table 2 summarizes the calculated values of the removal efficiency (%) of each sample at 410 and 590 min, and the removal efficiency (%) of each sample at 410 min is displayed in Figure 2c. The acetaldehyde removal efficiency of Fe-TiO₂ at 410 min increased significantly from that of TiO₂ (16.90%) when the Fe-TiO₂ sample was annealed at 300 °C (92.88%), and the efficiency was further increased upon the annealing of the Fe-TiO₂ sample at 375 °C (100%). On the other hand, as the annealing temperature increased above 375 °C, the enhancement effect of Fe-loading on the photocatalytic activity of TiO₂ for acetaldehyde removal under visible light irradiation became less pronounced. In particular, a significant reduction of the enhancement effect of Fe-loading was observed when the annealing temperature was higher than 450 °C. The selectivity of CO₂ was calculated for each sample as follows in Equation (3):

$$\frac{\text{The number of gaseous CO}_2 \text{ molecules evolved with each sample for each time}}{\text{(The number of removed acetaldehyde molecules with sample for each time)} \times 2} \times 100 \quad (3)$$

Table 2. Removal efficiencies for acetaldehyde determined after 410 min and 590 min of visible light irradiation in the presence of TiO₂, and Fe-TiO₂-300, -375, -450, -525, and -750.

	Acetaldehyde removal efficiency at 410 min (%)	Acetaldehyde removal efficiency at 590 min (%)
AS-received TiO ₂	16.90	17.84
Fe-TiO ₂ -300	92.88	100
Fe-TiO ₂ -375	100	100
Fe-TiO ₂ -450	87.50	100
Fe-TiO ₂ -525	43.31	56.69
Fe-TiO ₂ -750	41.35	56.73

The denominator corresponds to the number of CO₂ molecules generated by the total oxidation of the removed acetaldehyde; the total oxidation of 1 mol of acetaldehyde generates 2 mol of CO₂. Figure 2d shows that the CO₂ selectivity of the photocatalytic removal of acetaldehyde on the TiO₂ surface was also increased by Fe-loading and subsequent annealing. In addition, the enhancement effect of Fe-loading on the CO₂ selectivity also depended on the annealing temperature, similarly to the case of the acetaldehyde removal efficiency. The enhancement effects of Fe-loading on the CO₂ selectivity were most pronounced when the Fe-TiO₂ sample was annealed at 375 °C, whereas the effects became significantly less pronounced when the Fe-TiO₂ particles were annealed at higher temperatures (525 and 750 °C).

2.3. Further Analyses (UV Diffuse Reflectance Spectrophotometry (UV-DRS), Photoluminescence (PL), XPS, and TOF-SIMS)

The Fe-TiO₂-375 samples exhibited the highest photocatalytic activity in terms of both acetaldehyde removal and CO₂ evolution under visible light irradiation among the five Fe-TiO₂ samples (Fe-TiO₂-300, -375, -450, -525, and -750). The enhancement effects of Fe-loading on the photocatalytic activity of TiO₂ were reduced with increasing annealing temperature, and in particular, annealing at temperatures higher than 450 °C led to a significant reduction of the photocatalytic activity of Fe-TiO₂. In order to understand the annealing temperature dependency of the enhancement effects of Fe-loading, three representative samples (Fe-TiO₂-375, -525, and -750) were further analyzed by UV-DRS, PL, XPS, and TOF-SIMS.

The UV-vis reflectance of each sample was measured, and the obtained reflectance values were converted into values corresponding to the absorption values based on the Kubelka–Munk function [31–33] (Figure 3a). The UV-vis reflectance of the TiO₂ samples was also measured, and the values obtained using the Kubelka–Munk function are displayed in Figure 3a for comparison. The optical band gap of each sample can be determined by obtaining the X-axis intercept values of the extrapolated straight line of each Kubelka–Munk plot, and the optical band gap of TiO₂ was determined to be ~3.01 eV. The optical band gap of TiO₂ was reduced upon the Fe-loading and subsequent annealing (Figure 3a), and higher temperature annealing at 750 °C reduced the optical band gap a little further than in the cases of annealing at 375 and 525 °C. However, the modification effects on the optical band gap of TiO₂ did not seem to be significant; the band gap value of the Fe-TiO₂-750 sample was determined to be ~2.96 eV. In addition, the optical band gap changes upon Fe-loading, and the annealing did not correlate to the annealing temperature dependency of the modification effects on the photocatalytic activity of the Fe-TiO₂ samples; Fe-TiO₂-375 exhibited significantly higher photocatalytic activity than Fe-TiO₂-525 and -750, but the band gap reduction was most pronounced for the case of the Fe-TiO₂-750 sample. We would also like to mention that the optical band gaps of other synthesized Fe-TiO₂ samples (Fe-TiO₂-300, -450, and -525) were also determined, and the variation among all the synthesized samples and pristine TiO₂ were only marginal (Supporting information). These results indicate that the modification effects on the photocatalytic activity and its annealing temperature dependency cannot be simply explained by the optical band gap reduction due to Fe-loading and thermal annealing.

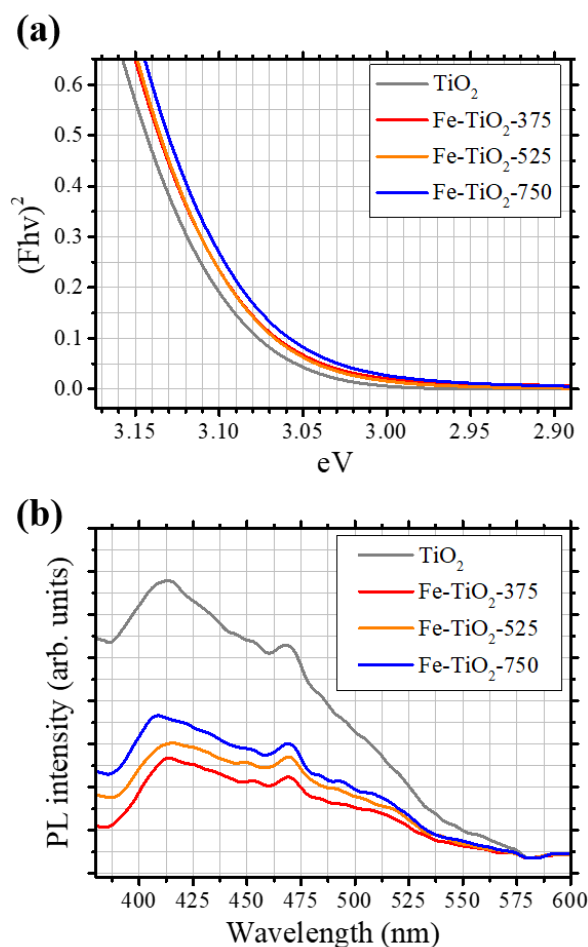


Figure 3. Results of UV diffuse reflectance spectrophotometry (UV-DRS) and photoluminescence (PL) analyses. (a) Kubelka–Munk plots of the results of UV-DRS measurements with TiO_2 and $Fe-TiO_2$ -375, -525, and -750. (b) PL signal measured with TiO_2 and $Fe-TiO_2$ -375, -525, and -750 samples.

Figure 3b shows photoluminescence (PL) spectra of four samples (TiO_2 and $Fe-TiO_2$ -375, -525, and -750). The PL intensities of three $Fe-TiO_2$ samples were significantly lower than that of TiO_2 , and $Fe-TiO_2$ -375 showed the lowest PL intensity among the three $Fe-TiO_2$ samples. The PL signal from each sample is related to the separation efficiency of the electron-hole pairs under light excitation. The energy of the irradiating light was absorbed by each sample, and electron-hole pairs were generated (electrons in the conduction band and holes in the valence band). When the light-induced electron-hole pairs are recombined, light can be emitted and detected as a PL signal. Thus, the weaker the PL signal, the higher the efficiency of the electron-hole separation (less recombination of electron-hole pairs took place). The PL analysis results indicated that Fe-loading can significantly improve the electron-hole separation efficiency, and the positive effects of Fe-loading on the charge separation efficiency depended on the annealing temperature; the effects were most pronounced upon the 375 °C-annealing of $Fe-TiO_2$, whereas increased annealing temperatures (>375 °C, e.g., 525 and 750 °C) resulted in the reduction of the enhancement of the charge separation efficiency by Fe-loading.

Later, three $Fe-TiO_2$ samples ($Fe-TiO_2$ -375, -525, and -750) were analyzed by two surface sensitive analysis techniques (XPS and TOF-SIMS), and the results are shown in Figures 4 and 5. Figure 4a–c show the Ti 2p, Fe 2p, and Al 2p core-level XPS spectra, respectively, of the three $Fe-TiO_2$ samples. The intensity of each XPS spectrum was normalized to the respective Ti 2p peak intensity. The binding energy of the Ti 2p_{3/2} peaks of all three samples were ~458.7 eV, corresponding to Ti^{4+} states [34–36], and the peak shapes and positions for the three samples were almost identical to each other (Figure 4a). An Al 2p core-level XPS peak centered at ~75 eV was also observed for all three samples (Figure 4b),

attributed to the existence of the alumina shell on the as-received TiO_2 particles. Note that alumina shells are generally considered to be required to increase the compatibility of TiO_2 with plastics or binders forming more uniform composite functional structures. In Supporting information, the Ti 2p and Al 2p core-level XPS spectra of the as-received TiO_2 are displayed together with those of the three Fe- TiO_2 samples (Fe- TiO_2 -375, -525, and -750). It is shown that the Ti 2p and Al 2p XPS spectra did not undergo significant changes upon the modification, excepting for the slight decrease in the Al 2p signal with the increase in the annealing temperature after Fe deposition from 375 to 750 °C (Supporting information). It is also worth noting that a significant Ti signal was detected together with the Al signal in the XPS analysis, although the surface of as-received TiO_2 was covered with alumina, indicating that either the alumina shell was very thin (~ 2 nm) or the surface of the TiO_2 was not completely covered by the alumina shell.

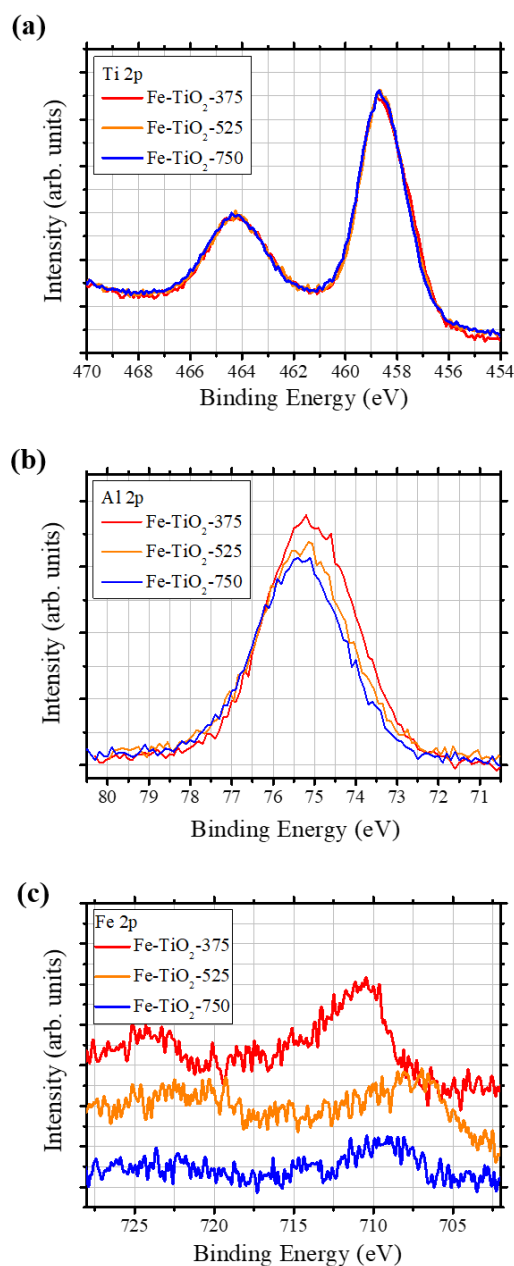


Figure 4. Results of XPS analysis. (a) Ti 2p, (b) Al 2p, and (c) Fe 2p core-level XPS spectra of Fe- TiO_2 -375, -525, and -750 samples.

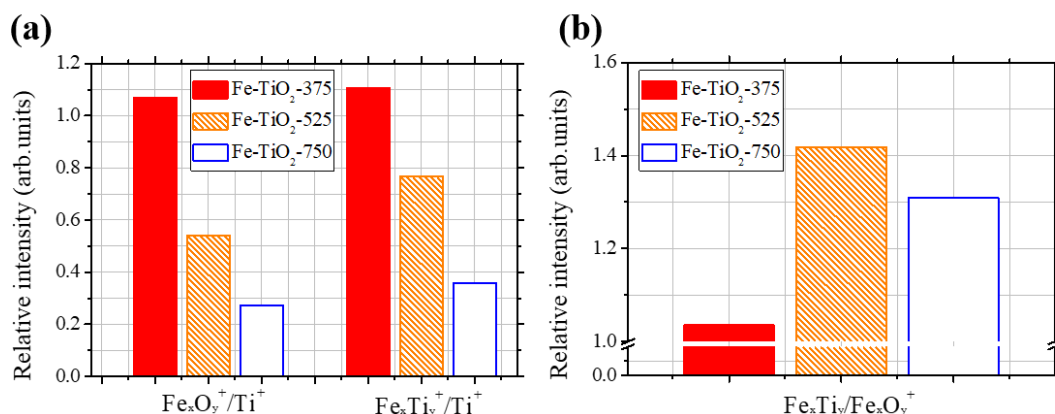


Figure 5. Results of TOF-SIMS analysis. (a) Secondary ion mass signals detected during TOF-SIMS analyses on Fe-TiO₂-375, -525, and -750 samples are compared. Secondary ion mass signals are categorized into two categories (FeO⁺ and FeTi⁺), where each category is the sum of the ion mass signals containing the respective ions (e.g., FeO⁺ is the sum of the ion mass signals containing Fe and O). The FeO⁺ and FeTi⁺ signals of each sample were divided by the respective Ti⁺ signal. (b) FeTi⁺ signals of three samples divided by the respective FeO⁺ signals are compared.

Upon Fe-loading and annealing, Fe 2p_{3/2} core-level XPS peaks appeared in the binding energy region of 713–703 eV (Figure 4c). The intensities of the Fe 2p core-level XPS spectra of the Fe-TiO₂ samples decreased with increasing annealing temperature, especially when the temperature was increased from 375 to 525 °C. This is similar to the case of the Al 2p core-level XPS spectra, where an intensity decrease was observed upon annealing at higher temperature, but the decrease in Fe 2p signal was more pronounced than that in the case of the Al 2p core-level. Along with the decrease in the Fe 2p signal intensity, a shift of the Fe 2p XPS peaks to the lower binding energy region was observed upon the higher temperature annealing; the Fe 2p_{3/2} peak of Fe-TiO₂-375 was centered at ~710 eV, whereas the center position of the Fe 2p_{3/2} peak of Fe-TiO₂-525 was at ~707 eV. The Fe 2p_{3/2} peak position of Fe-TiO₂-375 corresponded to oxidic Fe either in Fe(II) or Fe(III); by contrast, the peak positions of the two Fe-TiO₂ samples annealed at higher temperatures (Fe-TiO₂-525 and -750) corresponded to Fe atoms in the metallic state or Fe(I) state. Both the intensity decreases and the lower binding energy shift of the Fe 2p XPS peak with increasing annealing temperatures (>375 °C) seemed to be caused by the strong metal–support interaction (SMSI) of TiO₂ with the loaded Fe-oxide. The SMSI between the group VIII metals (e.g., Fe and Ni) and TiO₂ substrate had been reported, which varied the catalytic activities of the metals (metal oxides) of the group VIII atoms regarding Fischer–Tropsch (F-T) synthesis [37–39]. The SMSI between Fe-oxide and TiO₂ can result in (1) the encapsulation of the Fe-oxide by the TiO₂ (the scrambling up of the underlying TiO₂ [40–42] or interdiffusion of the Fe atoms into the TiO₂ substrate [43–46]) and (2) the reduction of the Fe-oxide by the charge transfer [43–46]. The surface structure changes of the Fe-TiO₂ samples upon higher temperature annealing due to SMSI effects were further evidenced by the TOF-SIMS analysis, the details of which are discussed below.

Three Fe-TiO₂ samples (Fe-TiO₂-375, -525, and -750) were further analyzed by TOF-SIMS using a Bi₃⁺ ion beam as a primary ion source. The intensities of the secondary ion signals measured by TOF-SIMS for each type of sample were normalized to the respective signal intensity of the Ti⁺ ion. All the measured secondary ion signals are summarized in Supporting information. The secondary mass signals other than Al⁺ and Fe⁺ were categorized into two groups, Fe_xO_y⁺ and Fe_xTi_y⁺, as shown in Figure 5a. The intensity of Fe_xO_y⁺ corresponds to the sum of the secondary ion signals containing Fe and O atoms, e.g., FeO⁺, FeO₂⁺, Fe₂O⁺, etc., whereas the Fe_xTi_y⁺ intensity shown in Figure 5a corresponds to the sum of the secondary ion signals containing Fe and Ti atoms. As the annealing temperature for the Fe-TiO₂ increased above 375 °C, the intensities of Fe_xO_y⁺ and Fe_xTi_y⁺ with respect to Ti⁺ gradually decreased, indicating the pronounced diffusion of Ti atoms to the top surface of the Fe-TiO₂ sample at higher temperatures (525 and 750 °C), which resulted in the higher coverage of the

loaded Fe-oxide surface by TiO₂. It is important to note that the decrease in the Fe_xO_y⁺/Ti⁺ signal with increasing annealing temperatures above 375 °C was more pronounced than in the Fe_xTi_y⁺/Ti⁺ case. Figure 5b compares the Fe_xTi_y⁺ signal to Fe_xO_y⁺ signal ratios of three samples (Fe-TiO₂-375, -525, and -750). An increase in the Fe_xTi_y⁺/Fe_xO_y⁺ signal ratio was notable as the annealing temperature was increased above 375 °C. The SIMS data only monitor the topmost surface structure, and therefore, intermixing between Fe and Ti in deeper layers is not fully reflected here. Nevertheless, these results indicate that the interaction between Fe and TiO₂ became stronger at higher temperatures (especially >375 °C), which can lead to more interdiffusion of Ti atoms to the loaded Fe-oxide and the reduction of the loaded Fe-oxide by TiO₂ (forming a compound such as FeTi₂O_{3-x}, in which Fe has an oxidation state of II or I). The SIMS analysis results were in line with the results of XPS analysis; both analysis results indicated the stronger SMSI effects of TiO₂ on the loaded Fe-oxide upon Fe-TiO₂ annealing at higher temperature (>375 °C). It is worth noting that both the SIMS and XPS analysis methods are surface-sensitive techniques, of which the typical analysis depths are ~2 nm and ~5 nm from the topmost surface, respectively.

We suggested the following scenario, which can reconcile all our observations of UV/vis, PL, XPS, SIMS, and the temperature dependency of the enhancement effects of Fe-loading on the photocatalytic activity of Fe-TiO₂ samples (Figure 6a). The electron-hole pairs were generated upon photon absorption. Electrons in the conduction band (or holes in the valence band) can transfer into Fe(III) atoms, reducing Fe(III) atoms into Fe(II) states (or oxidizing Fe(III) atoms into Fe(IV) states). If the Fe atoms in Fe(II) states (or Fe(IV) states) were available to the oxygen molecules (or water) adsorbed on the surface, electrons (or holes) could further transfer into oxygen molecules (or water), generating O₂⁻ ions (or OH radicals), and then the Fe atoms would return to the original Fe(III) states (Figure 6a). When these processes take place, the electron-hole separation efficiency of the Fe-TiO₂ samples under light irradiation can be improved, which can lead to the increased photocatalytic activity of Fe-TiO₂.

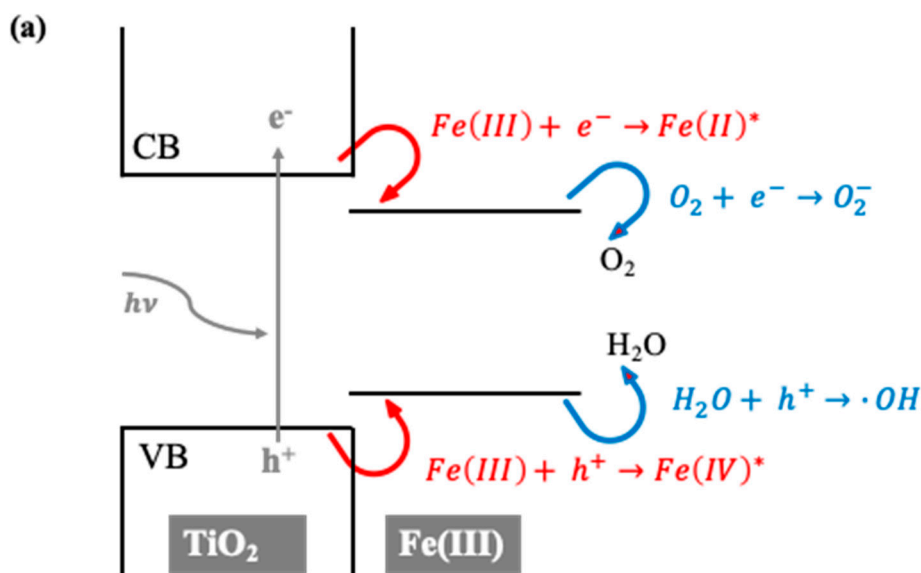


Figure 6. Cont.

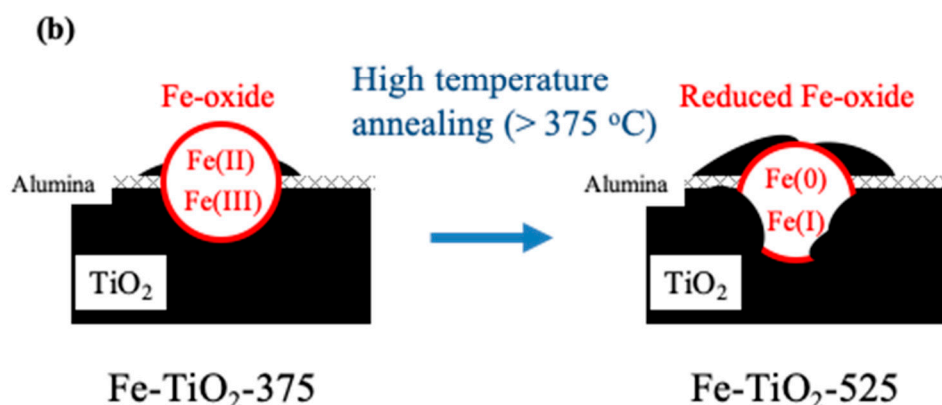


Figure 6. The suggested scenario. Schematic depictions of (a) the suggested scenario that explains the surface structure changes associated with higher temperature annealing and (b) the annealing temperature dependency of the photocatalytic activity of the Fe-TiO₂ sample.

The stronger SMSI effect of TiO₂ at higher temperatures (525 and 750 °C) not only facilitated the scrambling up of loaded Fe-oxide by the underlying TiO₂ but also resulted in the reduction of the loaded Fe atoms by the inter-diffusion of metal atoms between the TiO₂ and oxidized Fe structure (Figure 6b) [43–46]. The former effect made Fe atoms unavailable to the adsorbed oxygen or water molecules, while the latter made the charge transfer from TiO₂ to Fe atoms difficult [47,48]. That is to say, the effects of the stronger SMSI between TiO₂ and the loaded Fe-oxide at higher temperature resulted in the decrease in the charge separation efficiency of Fe-TiO₂, although, in our case study, the reduction of the oxidation states of the Fe atoms seemed to be more critical for decreasing the charge separation efficiency, and photocatalytic activity of Fe-TiO₂ upon higher temperature annealing (>375 °C).

2.4. Large-Scale Production of Catalysts and Their Potential Applications

Finally, we explored the potential applications of the Fe-TiO₂-375 particles. Firstly, we compared the photocatalytic activity of the Fe-TiO₂-375 sample with that of the Fe-loaded (0.1 wt% of Fe) commercial TiO₂ particles (P25, Evonik) annealed at 750 °C, hereafter denoted as Fe-P25-750. Previously, the Fe-P25-750 sample has been proven to exhibit the highest photocatalytic activity regarding acetaldehyde degradation under visible light irradiation among the P25 samples modified by the tr-CVD of Fe-oxide and thermal annealing [28]. The Fe-P25-750 sample containing 0.1 wt% of Fe was prepared via the tr-CVD of Fe-oxide on commercially available TiO₂ (P25, Evonik) and subsequent annealing at 750 °C, as described in the literature [28]. The photocatalytic removal of acetaldehyde on the surface of Fe-P25-750 was performed under the same conditions as in the Fe-TiO₂-375 case (Figure 7a,b). The Fe-P25-750 sample exhibited slightly better photocatalytic performance in terms of acetaldehyde removal and CO₂ evolution compared to the Fe-TiO₂-375 sample under the same conditions; a 100% removal efficiency for acetaldehyde was achieved by 370 min of visible light irradiation on the surface of Fe-P25-750, whereas a 100% removal efficiency was achieved on the surface of Fe-TiO₂-375 by 410 min of visible light irradiation. However, one should note that the TiO₂ used as a base material for Fe-TiO₂-375 in this work was produced via a sulfuric acid method, and its price (3 USD/g) is much lower than that of the P25 (50–70 USD/g). In addition, the modification process for the Fe-TiO₂-375 consumed much less energy than that for Fe-P25-750, owing to the lower temperature of the thermal annealing process (375 °C vs. 750 °C). Thus, considering the lower production costs of the Fe-TiO₂-375 relative to Fe-P25-750 and their comparable photocatalytic activities under visible light irradiation, the Fe-TiO₂-375 sample seemed to be a more favorable choice for industrial applications than Fe-P25-750.

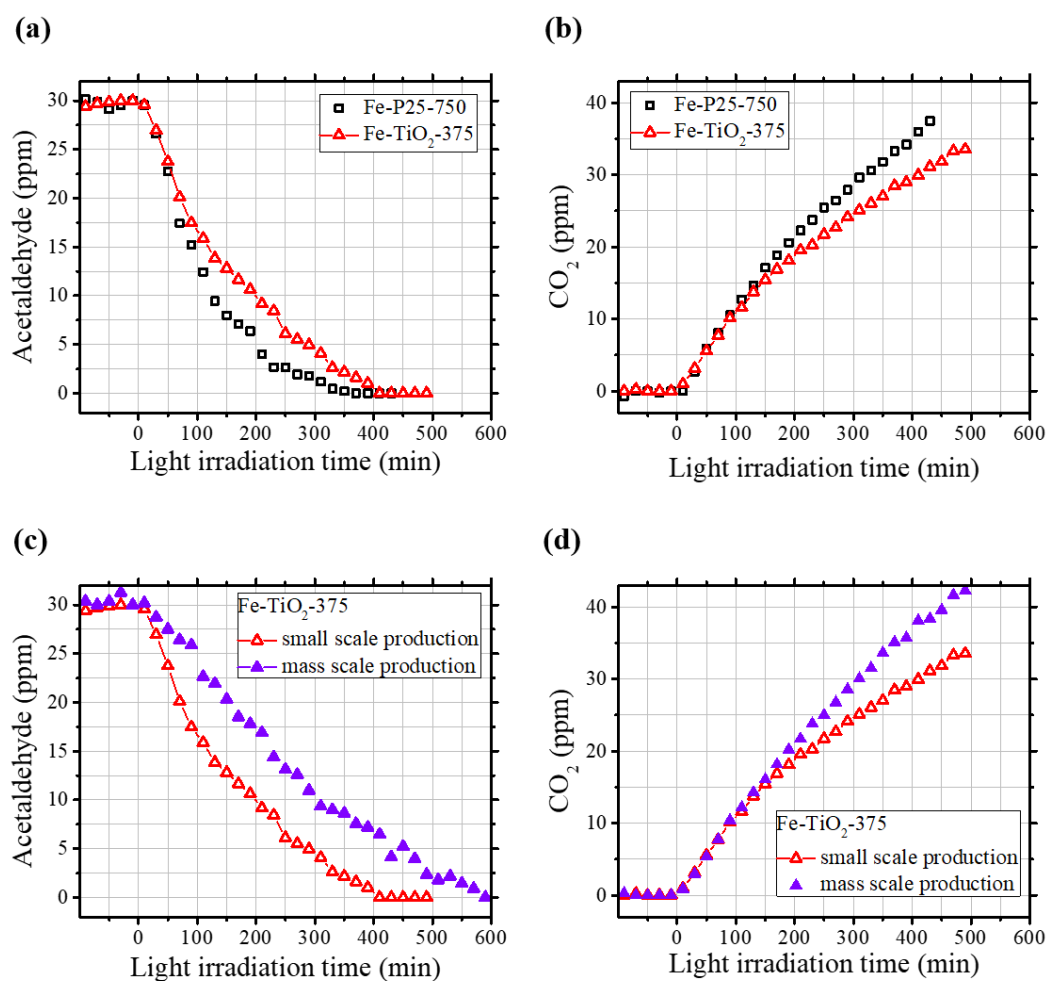


Figure 7. The results of the photocatalysis experiments (Fe-P25-750 and mass-produced Fe-TiO₂-375). Concentration changes of (a) acetaldehyde and (b) CO₂ as a function of the visible light irradiation (Table 2) and Fe-P25-750 samples. Concentration changes of (c) acetaldehyde and (d) CO₂ as a function of the visible light irradiation time in the presence of Fe-TiO₂-375 produced at small scale and mass-produced Fe-TiO₂-375.

We also tested the possibility of the mass production of Fe-TiO₂-375 photocatalysts. The Fe-TiO₂-375 samples were produced on a much larger scale; the amount of Fe-TiO₂-375 particles (8 kg) produced in one sequential tr-CVD and annealing process was 40 times greater than that in the aforementioned case (200 g). The photocatalytic activity of the mass-produced Fe-TiO₂-375 regarding acetaldehyde removal under the visible light irradiation was examined under the same conditions as for the case of the Fe-TiO₂-375 produced at a small scale (200 g per sequential tr-CVD and annealing process) (Figure 7c,d). The mass-produced Fe-TiO₂-375 exhibited a slightly lower efficiency of acetaldehyde removal (100% acetaldehyde removal at 600 min) than the Fe-TiO₂-375 sample produced at the small scale, which was most likely due to the existence of an induction period for the activity of the mass-produced samples due to the higher level of impurities, but it exhibited slightly higher efficiency in terms of CO₂ evolution. The results demonstrated the feasibility of the mass production of Fe-TiO₂-375 and its usability as a photocatalyst for air purification.

One of the potential applications of photocatalyst particles for improving outdoor or indoor air quality is putting those particles on the outside or inside walls of buildings. In order to explore this possibility, samples of Fe-TiO₂-375 particles were mixed with a commercially available paint and a surface hardening agent, and the mixtures were spread on a stainless use steel (SUS) plate and a cement block, respectively. Then, the photocatalytic removal of acetaldehyde under visible light in the presence

of each sample was examined under the same experimental conditions as in the aforementioned case (Fe-TiO₂-375 drop-casted on a SUS plate) (Figure 8a,b). For both cases, the initiation of the photocatalytic removal of acetaldehyde and CO₂ evolution was observed upon visible light irradiation (Figure 8a,b). It is interesting that both samples exhibited similar acetaldehyde removal efficiency, but the Fe-TiO₂-375 on the cement block showed a much higher efficiency of CO₂ evolution than the Fe-TiO₂ on the paint. This might be caused by the different natures of the adhesive materials between the two samples, but further systematic investigations are needed to reveal the effects of the adhesive materials on the photocatalytic activity of TiO₂-based particles. Nevertheless, it is worth noting that the Fe-TiO₂-375 particles can exhibit their photocatalytic activity under visible light irradiation after being mixed with other adhesive materials, which makes them applicable for air purification in outdoor or indoor environments.

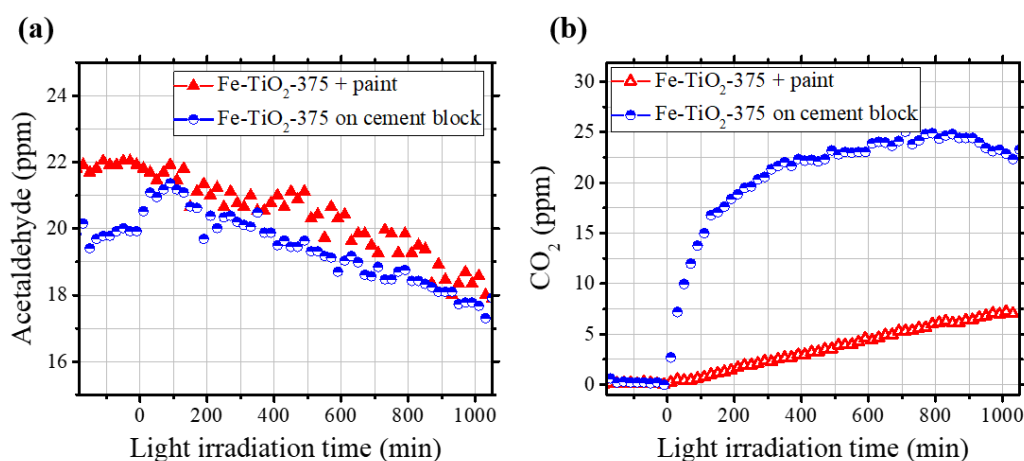


Figure 8. The results of the photocatalysis experiments (Fe-TiO₂-375 mixed with paint or adhesive materials). Concentration changes of (a) acetaldehyde and (b) CO₂ as a function of the visible light irradiation time in the presence of Fe-TiO₂-375 mixed with paint or a surface hardening agent and spread on a stainless steel surface or on a cement block, respectively.

3. Materials and Methods

3.1. Preparation of Photocatalysts

3.1.1. Small-Scale Production

FeO_x/TiO₂ photocatalysts were prepared by a temperature-regulated chemical vapor deposition (tr-CVD) method. Commercial titanium dioxide (TiO₂), bought from Lomo Billions, China, was used as a substrate. Bis(cyclopentadienyl)iron (Ferrocene, Fe(Cp)₂, Sigma Aldrich, USA) was used as a metal precursor, whereas oxygen and water in ambient air were used as the oxidizing agent. Two hundred grams of TiO₂ was mixed with 0.667 g of Fe(Cp)₂ (weight ratio of 300:1), and the mixture was placed in a quartz beaker (250 mL). Our previous studies showed that Fe-loading of less than 2% can have a significant enhancement effect on photocatalytic activity [28]. We used a different Fe-loading here, and the Fe-loading of 0.4 wt% prepared by a 1:300 ratio of TiO₂ and Fe(Cp)₂ resulted in better CO₂ selectivity, even though the acetaldehyde removal rate appeared to be less sensitive to the Fe-loading in this range (Supporting information). Thus, we concentrated on the Fe-loading of 0.4 wt% in the present work. The top part of the quartz beaker was covered with aluminum foil, and the gap between the beaker and aluminum foil was sealed with polyimide (PI) tape. The beaker was located in a box furnace (DMF-3T, U1TECH, Hwaseong, Korea) with an internal volume of 3 L. The temperature was increased to 60 °C and kept at 60 °C for 1 h for the evaporation of the Fe(CP)₂. After 1 h, the temperature was increased to 200 °C, and this temperature was maintained for 1 h to oxidize the Fe(Cp)₂ on the surface of TiO₂. The aluminum foil and PI tape were removed after the beaker was cooled down to room

temperature. Then, the tr-CVD-prepared samples were further annealed at various temperatures (300, 375, 450, 525, and 750 °C) for 2 h under ambient conditions. Hereafter, the Fe-oxide-loaded TiO₂ samples prepared via the tr-CVD of Fe-compounds and subsequent annealing at various temperatures are referred as Fe-TiO₂-annealing temperature, e.g., Fe-TiO₂-375 for 375 °C-annealed Fe-deposited TiO₂ sample, whereas TiO₂ is referred to as the as-received TiO₂.

3.1.2. Large-Scale Production

For the mass production of the Fe-deposited TiO₂ photocatalysts, a box furnace (PMF27, LAB HOUSE, Seoul, Korea) with a larger internal volume (27 L) was used, and the quartz beaker was replaced by an alumina crucible (size, 135 mm × 135 mm × 60 mm). Eight kilograms of TiO₂ was mixed with 27 g of Fe(Cp)₂ for 30 min using a cement mixer (DCM-300R, DCM corporation, Yangsan, Korea). The mixture of TiO₂ and Fe(Cp)₂ was distributed in the alumina crucibles (15 EA). The top of each alumina crucible was covered with an alumina lid, and the gap between the crucible and the lid was sealed with PI tape. Then, the crucibles were placed in the box furnace (internal volume of 27 L), and the tr-CVD of Fe-oxide on TiO₂ particles was initiated by increasing the temperature in the same manner as in the aforementioned case (small-scale production, 1 h of 60 °C-heating followed by 1 h of 200 °C-heating). After the tr-CVD of the Fe-compound on the TiO₂ particles, the crucibles were cooled down until the temperature reached room temperature, and then the lids and PI tape were removed from the tops of all the crucibles. Then, the Fe-TiO₂ was further annealed at 375 °C for 2 h under ambient conditions using the same furnace (27 L-box furnace).

3.2. Characterization of Photocatalysts

The amounts of the Fe loading of Fe-TiO₂ were determined by inductively coupled plasma optical emission spectroscopy (ICP-OES, Varian, Agilent, Santa Clara, California, USA). Three samples (TiO₂, and Fe-TiO₂-375 and -750) were selected for transmission electronic microscopy (TEM), X-ray diffraction (XRD), and surface area analyses. Structural images of three samples were obtained using TEM (JEM-3010, Jeol, Japan). The crystallinity of each sample was studied by obtaining X-ray diffraction (XRD) patterns using a diffractometer (Ultima IV, Rigaku, Tokyo, Japan) and Cu K α radiation. The N₂ adsorption/desorption isotherm (3Flex, Micromeritics, Norcross, Georgia, USA) of each sample was obtained, and the surface area of each sample was determined using the Brunauer–Emmett–Teller (BET) method.

TiO₂ and Fe-TiO₂-375, Fe-TiO₂-525, and Fe-TiO₂-750 samples were characterized with a UV-Vis diffuse reflectance spectrophotometer (UV-DRS, UV-3600, SHIMADZU, Japan) and photoluminescence spectrometer (FS-2, SCINCO, Seoul, Korea). The surfaces of four samples (TiO₂, and Fe-TiO₂-375, -525, and -750) were also analyzed by X-ray photoelectron spectroscopy (XPS). XPS measurements were carried out under ultra-high vacuum conditions with a base pressure of 5.0×10^{-10} Torr. The XPS spectrum of each sample was collected by a concentric hemispherical analyzer (CHA, PHOIBOS-HSA3500, SPECS, Berlin, Germany) in a fixed pass energy mode (30 eV), and Mg K α radiation (1253.6 eV) was used.

Time-of-flight SIMS (TOF-SIMS) analyses were performed for the three selected Fe-TiO₂ samples (Fe-TiO₂-375, -525, and -750) using a TOF-SIMS 5 (ION-TOF GmbH, Muenster, Germany). The instrument was equipped with a Bi liquid metal ion gun aligned along the axes at 45° to the surface of the sample. For SIMS analysis, Bi₃⁺ was used as the primary ion with an acceleration voltage of 30 keV, and the secondary positive ions emitted from the surface of the sample were analyzed with the TOF mass spectrometer. The pressed pellet of each sample was mounted on the sample stage of the chamber using carbon tape. A 500 $\mu\text{m} \times 500 \mu\text{m}$ area of the sample was analyzed, and each SIMS spectrum was obtained by accumulating signals from 30 scans. The mass scale of the SIMS experiment was calibrated using H⁺, CH₃⁺, C₂H₅⁺, C₃H₇⁺, and C₄H₉⁺.

3.3. Photocatalytic Decomposition of Acetaldehyde

The photocatalytic removal of acetaldehyde on the surface of TiO₂ samples (TiO₂ and Fe-TiO₂-300, -375, -450, -525, and -750) was studied under visible light irradiation using a batch-type reactor (Supporting information). A high vacuum chamber (base pressure of $\sim 2.0 \times 10^{-5}$ Torr, reactor volume of ~ 5.3 L) was used as a reactor, and it was equipped with a convection vacuum gauge (SUPER BEE, InstruTech, Longmont, Colorado, USA), oil rotary (W2V40, WSA CO. LTD., Hwaseong, Korea), and turbomolecular pump (TMG 260P, PFEIFFER VACUUM Technology AG, Germany). The chamber was connected to the gas chromatograph (GC, HP 6890 series, Hewlett Packard) via $\frac{1}{4}$ " SUS lines equipped with an HP-PLOT/Q column (19095P-Q04, 30 m \times 0.530 mm \times 40 μ m, Agilent, Santa Clara, California, USA) and flame ionization detector (FID). Along the $\frac{1}{4}$ " SUS lines, a diaphragm pump (DA70EEAC, flow rate of 7 L/min, YLKTECH) was installed between the GC and chamber to circulate the gas through the reactor. Polytetrafluoroethylene (PTFE) tubes ($\frac{1}{4}$ "") were used for the inlet and outlet lines of the diaphragm pump to accommodate the vibration of the diaphragm pump. The top side of the chamber was composed of a quartz view port, which allowed the efficient transmission of light from the light source located on the outside of the chamber.

The thin film of each photocatalyst was prepared by drop-casting 0.15 g of each sample on a SUS (stainless steel) plate (6 \times 6 cm²) [28], and it was mounted on the sample stage of the chamber. After the sample mounting, the reactor was pumped down until the reactor pressure reached $\sim 2.0 \times 10^{-5}$ Torr, and then the reactor was filled with a gas mixture (total pressure of 760 Torr) consisting of H₂O, O₂, dry air, and acetaldehyde diluted with N₂ (201 mol ppm). Each gas was injected into the reactor using a leak valve while monitoring its partial pressure with the vacuum gauge. The composition of the total gas mixture corresponded to ambient air containing 30 ppm of acetaldehyde with a relative humidity (RH) of 33% at 25 °C. After the reactor was filled with the gas mixture, the diaphragm pump was turned on to circulate the gas mixture through the reactor. Every 10 min, 50 μ L of the gas mixture inside the reactor was injected into the GC to monitor the acetaldehyde and CO₂ concentration. Prior to the initiation of the GC analysis, the gas mixture in the reactor was pre-circulated by the diaphragm pump for 30 min in the dark to achieve a homogeneous gas composition throughout the reactor. The adsorption of acetaldehyde on each sample was monitored for 3 h in the dark. The blue LED lamp emitted visible light with a maximum intensity at 460 nm. The wavelength of the emitted light was in the range of 420–490 nm (Supporting information), and the distance between the blue LED and sample surface was 10 cm. The reactor temperature was kept at ~ 24 °C throughout the experiments by controlling the temperature of the laboratory using an air conditioning system. The standard deviation of the reactor temperature over 10 h was 0.32 °C (24.3 °C \pm 0.32 °C). We would like to mention that our testing method for the photocatalytic removal of acetaldehyde is different from the ISO standard method (ISO 22197-2:2011, details are provided in Supporting information). The main difference between our method and the ISO standard is that a batch-type reactor was used in this study, which is beneficial for examining the reaction rates compared to the flow-type reactor (ISO standard).

Additional photocatalytic experiments were performed with a selected Fe-TiO₂ sample (Fe-TiO₂-375) to demonstrate the potential applications of the Fe-loaded TiO₂ sample. For this purpose, samples of Fe-TiO₂-375 were mixed with a surface hardening agent (BUFFHARD, STEL corporation, Korea) and a paint (NOROO, Korea), and the resulting mixtures were loaded on a cement block (6 \times 6 cm²) and SUS plate (6 \times 6 cm²), respectively. The Fe-TiO₂-375 content in each mixture (Fe-TiO₂-375 mixed with surface hardening agents and Fe-TiO₂-375 mixed with paint) was 10 wt%, and 1 g of each mixture was loaded. The photocatalytic experiment with these samples was carried out in the same manner, and under the same conditions, as those performed with the TiO₂ thin films on SUS plates.

4. Conclusions

Commercial rutile TiO₂ particles (200–300 nm) whose surfaces were covered with a thin alumina shell were modified by the tr-CVD of Fe-oxide (0.4 wt%) and subsequent thermal annealing in the temperature range of 300–750 °C. The particle size and crystallinity of the rutile TiO₂ particles

were not changed by the modification. The photocatalytic performance of the TiO₂ in terms of acetaldehyde removal and CO₂ evolution under visible light irradiation was significantly enhanced by the modification. The enhancement effect of the Fe-loading was dependent on the annealing temperature (300~750 °C), and the effect was most pronounced at 375 °C. The enhancement effect decreased gradually as the annealing temperature increased above 375 °C, and in particular, the Fe-TiO₂-525 and Fe-TiO₂-750 samples showed significantly lower activity than the Fe-TiO₂-375 sample.

Three representative Fe-TiO₂ samples (Fe-TiO₂-375, -525, and -750) were further analyzed using various techniques, including two surface-sensitive methods (XPS and TOF-SIMS). The higher-temperature annealing (525 and 750 °C) led to the stronger metal support interactions of TiO₂ with the structure of oxidized Fe. It resulted in the reduction of the oxidation states of the loaded Fe-oxide as well as a decrease in the surface Fe-oxide available to the adsorbed molecules at the higher annealing temperature (>375 °C). These effects resulted in the decreased charge separation efficiency of the Fe-TiO₂ sample under light irradiation, which led to the reduction of the enhancement effect of Fe-loading on the photocatalytic activity of the Fe-TiO₂ sample.

Furthermore, we demonstrated that the amounts of Fe-TiO₂-375 sample produced in one sequential tr-CVD and annealing process can be easily increased up to 8 kg from 200 g. The mass-produced sample also exhibited photocatalytic activity regarding acetaldehyde removal under visible light that was comparable to that of the small-scale-produced Fe-TiO₂-375 sample. In addition, the Fe-TiO₂-375 particles exhibited noticeable photocatalytic activity regarding acetaldehyde removal under visible light after they were mixed with either paint or a surface-hardening agent and spread on the SUS or on a cement block. These results showed the high applicability of the Fe-modified rutile TiO₂ for applications for air purification in either outdoor or indoor environments.

Supplementary Materials: The following are available online at <http://www.mdpi.com/2073-4344/10/7/739/s1>. Figure S1: (a) Ti 2p and (b) Al 2p core-level XPS spectra of TiO₂ and Fe-TiO₂-375, -525, and -750 samples. Figure S2: Summary of all measured secondary ion signals. Figure S3: Concentration changes of (a) acetaldehyde and (b) CO₂ as a function of the visible light irradiation time in the presence of two different Fe-TiO₂ samples (0.4 wt% Fe-TiO₂-375 and 1.6 wt% Fe-TiO₂-375). Figure S4: Experimental set up of the batch type reactor for the measurement of photocatalytic activity. Figure S5: Intensity of blue light measured by using a luminance spectrophotometer (CL-500A, Konica Minolta, Japan).

Author Contributions: S.Y.K., data curation, formal analysis, investigation, and methodology; S.S., data curation and methodology; B.J.C., formal analysis and methodology; S.Z., formal analysis and investigation; H.O.S., data curation, validation, writing—original draft, and writing—review and editing; Y.D.K., conceptualization, funding acquisition, project administration, resources, and writing—review and editing. All authors have read and agreed to the published version of the manuscript.

Funding: This research was supported by the Basic Science Research Program through the National Research Foundation of Korea (NRF) funded by the Ministry of Education (2018R1D1A1B07040916) (2017R1D1A1B03034381) and a research grant from the Korea Basic Science Institute (D010100).

Conflicts of Interest: The authors declare no conflict of interest.

References

1. Shayegan, Z.; Lee, C.-S.; Haghghat, F. TiO₂ photocatalyst for removal of volatile organic compounds in gas phase—A review. *Chem. Eng. J.* **2018**, *334*, 2408–2439. [[CrossRef](#)]
2. Gaya, U.I.; Abdullah, A.H. Heterogeneous photocatalytic degradation of organic contaminants over titanium dioxide: A review of fundamentals, progress and problems. *J. Photochem. Photobiol. C* **2008**, *9*, 1–12. [[CrossRef](#)]
3. McCullagh, C.; Robertson, J.M.C.; Bahnemann, D.W.; Robertson, P.K.J. The application of TiO₂ photocatalysis for disinfection of water contaminated with pathogenic micro-organisms: A review. *Res. Chem. Intermed.* **2007**, *33*, 359–375. [[CrossRef](#)]
4. Zou, W.; Gao, B.; Ok, Y.S.; Dong, L. Integrated adsorption and photocatalytic degradation of volatile organic compounds (VOCs) using carbon-based nanocomposites: A critical review. *Chemosphere* **2019**, *218*, 845–859. [[CrossRef](#)] [[PubMed](#)]
5. Chatterjee, D.; Dasgupta, S. Visible light induced photocatalytic degradation of organic pollutants. *J. Photochem. Photobiol. C* **2005**, *6*, 186–205. [[CrossRef](#)]

6. Mo, J.; Zhang, Y.; Xu, Q.; Lamson, J.J.; Zhao, R. Photocatalytic purification of volatile organic compounds in indoor air: A literature review. *Atmos. Environ.* **2009**, *43*, 2229–2246. [[CrossRef](#)]
7. Kampa, M.; Castanas, E. Human health effects of air pollution. *Environ. Pollut.* **2008**, *151*, 362–367. [[CrossRef](#)] [[PubMed](#)]
8. Berglund, B.; Brunekreef, B.; Knöppe, H.; Lindvall, T.; Maroni, M.; Mølhave, L.; Skov, P. Effects of Indoor air pollution on human health. *Indoor Air* **1992**, *2*, 2–25. [[CrossRef](#)]
9. Feron Victor, J.; Cassee Flemming, R.; Groten John, P.; van Vliet Petronella, W.; van Zorge Job, A. International issues on human health effects of exposure to chemical mixtures. *Environ. Health Perspect.* **2002**, *110*, 893–899. [[CrossRef](#)]
10. Lovreglio, P.; Carrus, A.; Iavicoli, S.; Drago, I.; Persechino, B.; Soleo, L. Indoor formaldehyde and acetaldehyde levels in the province of Bari, South Italy, and estimated health risk. *J. Environ. Monit.* **2009**, *11*, 955–961. [[CrossRef](#)]
11. Cavalcante, R.M.; Seyffert, B.H.; D’Oca, M.G.M.; Nascimento, R.F.; Campelo, C.S.; Pinto, I.S.; Anjos, F.B.; Costa, A.H.R. Exposure Assessment for Formaldehyde and Acetaldehyde in the Workplace. *Indoor Built Environ.* **2005**, *14*, 165–172. [[CrossRef](#)]
12. Saleh, T.A.; Gondal, M.A.; Drmash, Q.A.; Yamani, Z.H.; Al-yamani, A. Enhancement in photocatalytic activity for acetaldehyde removal by embedding ZnO nano particles on multiwall carbon nanotubes. *Chem. Eng. J.* **2011**, *166*, 407–412. [[CrossRef](#)]
13. Chang, C.-A.; Ray, B.; Paul, D.K.; Demydov, D.; Klabunde, K.J. Photocatalytic reaction of acetaldehyde over SrTiO₃ nanoparticles. *J. Mol. Catal. A Chem.* **2008**, *281*, 99–106. [[CrossRef](#)]
14. Arai, T.; Horiguchi, M.; Yanagida, M.; Gunji, T.; Sugihara, H.; Sayama, K. Complete oxidation of acetaldehyde and toluene over a Pd/WO₃ photocatalyst under fluorescent- or visible-light irradiation. *Chem. Commun.* **2008**, 5565–5567. [[CrossRef](#)]
15. Arai, T.; Yanagida, M.; Konishi, Y.; Iwasaki, Y.; Sugihara, H.; Sayama, K. Efficient complete oxidation of acetaldehyde into CO₂ over CuBi₂O₄/WO₃ composite photocatalyst under visible and UV light Irradiation. *J. Phys. Chem. C* **2007**, *111*, 7574–7577. [[CrossRef](#)]
16. Wu, H.B.; Hng, H.H.; Lou, X.W. Direct Synthesis of Anatase TiO₂ Nanowires with Enhanced Photocatalytic Activity. *Adv. Mater.* **2012**, *24*, 2567–2571. [[CrossRef](#)] [[PubMed](#)]
17. Liu, G.; Sun, C.; Yang, H.G.; Smith, S.C.; Wang, L.; Lu, G.Q.; Cheng, H.-M. Nanosized anatase TiO₂ single crystals for enhanced photocatalytic activity. *Chem. Commun.* **2010**, *46*, 755–757. [[CrossRef](#)] [[PubMed](#)]
18. Yu, J.; Yu, H.; Cheng, B.; Zhao, X.; Zhang, Q. Preparation and photocatalytic activity of mesoporous anatase TiO₂ nanofibers by a hydrothermal method. *J. Photochem. Photobiol. A* **2006**, *182*, 121–127. [[CrossRef](#)]
19. Lv, K.; Yu, J.; Cui, L.; Chen, S.; Li, M. Preparation of thermally stable anatase TiO₂ photocatalyst from TiOF₂ precursor and its photocatalytic activity. *J. Alloy. Compd.* **2011**, *509*, 4557–4562. [[CrossRef](#)]
20. Li, D.; Haneda, H.; Hishita, S.; Ohashi, N. Visible-Light-Driven N–F–Codoped TiO₂ Photocatalysts. 2. Optical Characterization, Photocatalysis, and Potential Application to Air Purification. *Chem. Mater.* **2005**, *17*, 2596–2602. [[CrossRef](#)]
21. In, S.; Orlov, A.; Berg, R.; García, F.; Pedrosa-Jimenez, S.; Tikhov, M.S.; Wright, D.S.; Lambert, R.M. Effective Visible Light-Activated B-Doped and B,N-Codoped TiO₂ Photocatalysts. *J. Am. Chem. Soc.* **2007**, *129*, 13790–13791. [[CrossRef](#)] [[PubMed](#)]
22. Seh, Z.W.; Liu, S.; Low, M.; Zhang, S.-Y.; Liu, Z.; Mlayah, A.; Han, M.-Y. Janus Au-TiO₂ Photocatalysts with Strong Localization of Plasmonic Near-Fields for Efficient Visible-Light Hydrogen Generation. *Adv. Mater.* **2012**, *24*, 2310–2314. [[CrossRef](#)] [[PubMed](#)]
23. Nahar, M.S.; Hasegawa, K.; Kagaya, S. Photocatalytic degradation of phenol by visible light-responsive iron-doped TiO₂ and spontaneous sedimentation of the TiO₂ particles. *Chemosphere* **2006**, *65*, 1976–1982. [[CrossRef](#)] [[PubMed](#)]
24. Niu, Y.; Xing, M.; Zhang, J.; Tian, B. Visible light activated sulfur and iron co-doped TiO₂ photocatalyst for the photocatalytic degradation of phenol. *Catal. Today* **2013**, *201*, 159–166. [[CrossRef](#)]
25. Li, L.; Yan, J.; Wang, T.; Zhao, Z.-J.; Zhang, J.; Gong, J.; Guan, N. Sub-10 nm rutile titanium dioxide nanoparticles for efficient visible-light-driven photocatalytic hydrogen production. *Nat. Commun.* **2015**, *6*, 5881. [[CrossRef](#)]
26. Neubert, S.; Pulisova, P.; Wiktor, C.; Weide, P.; Mei, B.; Guschin, D.A.; Fischer, R.A.; Muhler, M.; Beranek, R. Enhanced photocatalytic degradation rates at rutile TiO₂ photocatalysts modified with redox co-catalysts. *Catal. Today* **2014**, *230*, 97–103. [[CrossRef](#)]

27. Ohno, T.; Murakami, N.; Tsubota, T.; Nishimura, H. Development of metal cation compound-loaded S-doped TiO₂ photocatalysts having a rutile phase under visible light. *Appl. Catal. A* **2008**, *349*, 70–75. [[CrossRef](#)]
28. Saqlain, S.; Cha, B.J.; Kim, S.Y.; Ahn, T.K.; Park, C.; Oh, J.-M.; Jeong, E.C.; Seo, H.O.; Kim, Y.D. Visible light-responsive Fe-loaded TiO₂ photocatalysts for total oxidation of acetaldehyde: Fundamental studies towards large-scale production and applications. *Appl. Surf. Sci.* **2020**, *505*, 144160. [[CrossRef](#)]
29. Arai, T.; Horiguchi, M.; Yanagida, M.; Gunji, T.; Sugihara, H.; Sayama, K. Reaction mechanism and activity of WO₃-catalyzed photodegradation of organic substances promoted by a CuO cocatalyst. *J. Phys. Chem. C* **2009**, *113*, 6602–6609. [[CrossRef](#)]
30. Arai, T.; Yanagida, M.; Konishi, Y.; Iwasaki, Y.; Sugihara, H.; Sayama, K. Promotion effect of CuO co-catalyst on WO₃-catalyzed photodegradation of organic substances. *Catal. Commun.* **2008**, *9*, 1254–1258. [[CrossRef](#)]
31. López, R.; Gómez, R. Band-gap energy estimation from diffuse reflectance measurements on sol-gel and commercial TiO₂: A comparative study. *J. Sol-Gel Sci. Technol.* **2012**, *61*, 1–7. [[CrossRef](#)]
32. Nobbs, J.H. Kubelka—Munk Theory and the Prediction of Reflectance. *Rev. Prog. Color. Relat. Top.* **1985**, *15*, 66–75. [[CrossRef](#)]
33. Ishibai, Y.; Sato, J.; Nishikawa, T.; Miyagishi, S. Synthesis of visible-light active TiO₂ photocatalyst with Pt-modification: Role of TiO₂ substrate for high photocatalytic activity. *Appl. Catal. B* **2008**, *79*, 117–121. [[CrossRef](#)]
34. Gonbeau, D.; Guimon, C.; Pfister-Guillouzo, G.; Levasseur, A.; Meunier, G.; Dormoy, R. XPS study of thin films of titanium oxysulfides. *Surf. Sci.* **1991**, *254*, 81–89. [[CrossRef](#)]
35. Biener, J.; Bäumer, M.; Wang, J.; Madix, R.J. Electronic structure and growth of vanadium on TiO₂(110). *Surf. Sci.* **2000**, *450*, 12–26. [[CrossRef](#)]
36. Mayer, J.T.; Diebold, U.; Madey, T.E.; Garfunkel, E. Titanium and reduced titania overlayers on titanium dioxide(110). *J. Electron Spectrosc. Relat. Phenom.* **1995**, *73*, 1–11. [[CrossRef](#)]
37. Madhusudhan Rao, P.; Viswanathan, B.; Viswanath, R.P. Strong metal support interaction state in the Fe/TiO₂ system—An XPS study. *J. Mater. Sci.* **1995**, *30*, 4980–4985. [[CrossRef](#)]
38. van de Loosdrecht, J.; van der Kraan, A.M.; van Dillen, A.J.; Geus, J.W. Metal-support interaction: Titania-supported nickel-iron catalysts. *Catal. Lett.* **1996**, *41*, 27–34. [[CrossRef](#)]
39. Junzhuo, D.; Dezheng, W.; Xuming, W.; Runsheng, Z.; Hongli, W. Interactions in the Fe/TiO₂(110) system. *Surf. Sci.* **1991**, *249*, 213–222. [[CrossRef](#)]
40. Bonanni, S.; Aït-Mansour, K.; Brune, H.; Harbich, W. Overcoming the Strong Metal–Support Interaction State: CO Oxidation on TiO₂(110)-Supported Pt Nanoclusters. *ACS Catal.* **2011**, *1*, 385–389. [[CrossRef](#)]
41. Bowker, M.; Stone, P.; Morrall, P.; Smith, R.; Bennett, R.; Perkins, N.; Kvon, R.; Pang, C.; Fourre, E.; Hall, M. Model catalyst studies of the strong metal–support interaction: Surface structure identified by STM on Pd nanoparticles on TiO₂(110). *J. Catal.* **2005**, *234*, 172–181. [[CrossRef](#)]
42. Gao, Y.; Liang, Y.; Chambers, S.A. Thermal stability and the role of oxygen vacancy defects in strong metal support interaction — Pt on Nb-doped TiO₂(100). *Surf. Sci.* **1996**, *365*, 638–648. [[CrossRef](#)]
43. Pal, B.; Sharon, M.; Nogami, G. Preparation and characterization of TiO₂/Fe₂O₃ binary mixed oxides and its photocatalytic properties. *Mater. Chem. Phys.* **1999**, *59*, 254–261. [[CrossRef](#)]
44. Gao, B.; Yang, C.; Chen, J.; Ma, Y.; Xie, J.; Zhang, H.; Wei, L.; Li, Q.; Du, J.; Xu, Q. Ferromagnetic photocatalysts of FeTiO₃–Fe₂O₃ nanocomposites. *RSC Adv.* **2017**, *7*, 54594–54602. [[CrossRef](#)]
45. Ren, Z.-S.; Hu, X.-j.; Li, S.-Y.; Xue, X.-X.; Chou, K.-C. Interdiffusion in the Fe₂O₃-TiO₂ system. *Int. J. Miner. Metall. Mater.* **2013**, *20*, 273–278. [[CrossRef](#)]
46. Afonin, N.N.; Logacheva, V.A. Interdiffusion and phase formation in the Fe–TiO₂ thin-film system. *Semiconductors* **2017**, *51*, 1300–1305. [[CrossRef](#)]
47. Chang, S.-M.; Liu, W.-S. The roles of surface-doped metal ions (V, Mn, Fe, Cu, Ce, and W) in the interfacial behavior of TiO₂ photocatalysts. *Appl. Catal. B* **2014**, *156–157*, 466–475. [[CrossRef](#)]
48. Li, X.; Yue, P.-L.; Kutal, C. Synthesis and photocatalytic oxidation properties of iron doped titanium dioxide nanosemiconductor particles. *New J. Chem.* **2003**, *27*, 1264–1269. [[CrossRef](#)]

